M. Grosse, J. R. Santisteban, J. Bertsch, B. Schillinger, A. Kaestner, M. R. Daymond and *N. Kardjilov*

Investigations of the hydrogen diffusion and distribution in Zirconium by means of Neutron Imaging

Absorbed hydrogen degrades the mechanical properties of zirconium alloys used for nuclear fuel claddings. Not only the total amount of hydrogen absorbed in the cladding tube but also the zirconium hydride orientation and its distribution influence the toughness of the material. For instance, the so-called delayed hydride cracking is caused by the diffusive re-distribution of hydrogen into the dilative elastic strain field ahead of crack tips. The paper presents in-situ and ex-situ neutron imaging investigations of hydrogen uptake, diffusion and distribution in zirconium alloys used for claddings. An overview about results of in-situ experiments studying the hydrogen uptake in strained Zircaloy-4, as well as ex-situ investigations of the diffusion of hydrogen in cold rolled Zircaloy-2 and Zr-2.5 % Nb alloy depending on temperature, rolling direction and thermal treatment and of the hydrogen re-distribution in the β-phase of Zircaloy-4 during a Three-Point-Bending-Test at 600 °C are presented.

Neutronenradiographie- und -tomographieuntersuchungen der Wasserstoffdiffusion und -verteilung in Zirkonium. *Als Material für Brennstabhüllrohre in Leichtwassereaktoren werden Zirkonium-Legierungen verwendet. Wenn diese Wasserstoff aufnehmen, verschlechtern sich ihre mechanischen Eigenschaften. Dabei wird die Zähigkeit der Materialien nicht nur durch die Menge des absorbierten Wasserstoffs, sondern auch von der Orientierung und Verteilung der Hydride beeinflusst. Zum Beispiel ist der sogenannte verzögerte Wasserstoffbruch von der diffusionsgesteuerten Umverteilung des Wasserstoffs zum Gebiet vor einer Rissspitze verursacht, welches elastisch gedehnt ist. Dieser Artikel präsentiert Ergebnisse von in-situ Neutronenradiographie-Studien der Wasserstoffaufnahme in gedehnten Zircaloy-4-Proben, und ex-situ Untersuchungen zur Wasserstoffdiffusion in kaltgewalzten Zircaloy-2 und Zr-2.5 %Nb-Legierungen in Abhängigkeit von Temperatur, Walzrichtung und Wärmebehandlung sowie zur Umverteilung des Wasserstoffs in der β-Phase von Zircaloy-4 während eines Drei-Punkt-Biege-Test bei 600 °C.*

1 Introduction

Delayed hydride cracking (DHC) occurs at constant subcritical mechanical load after a holding time depending on temperature, load and hydrogen concentration. The phenomenology is intensively studied [1–8]. Hydrogen diffuses to the stress field ahead of a crack tip because the hydrogen chemical potential decreases in tensile strained zirconium. According to Varias [2] the chemical potential of hydrogen in solid solution μ^H is given:

$$\mu^H = \mu^{H,0} + \frac{\partial w}{\partial N^H} - W^H \tag{1}$$

$\mu^{H,0}$ is the free hydrogen potential in unstressed zirconium depending on the hydrogen concentration. w is the elastic energy of the zirconium, N^H the number of hydrogen atoms and W^H is the elastic work performed by the applied stresses.

The hydrogen enrichment ahead of a crack tip results in a reduction of toughness of this location with the consequences of progressing crack growth into this region. By the crack propagation, the residual stress of this region is released. The hydrogen chemical potential of this now unstrained position increases. The hydrogen chemical activity is now too high whereas at the newly formed strain region ahead of the new crack tip it is too low. Hydrogen has to diffuse from the former crack tip position to locations ahead of the new crack tip. The process starts again until failure of the cladding tube.

Less progress was achieved to model the mechanism of DHC. For this topic, the diffusion of hydrogen and the dependence of hydrogen chemical potential in zirconium alloys on the lattice strain have to be quantified.

Neutron imaging experiments can contribute improving the mechanistic understanding of the processes occurring during DHC in zirconium-based alloys. Because hydrogen has a very high and zirconium a very low total microscopic neutron cross-section σ_{total}, even low hydrogen concentrations can be detected in zirconium based materials. Therefore, the method becomes established and used to study hydrogen in zirconium alloys by various groups [9–21]. The relative fast and non-destructive neutron radiography investigations and the large penetration lengths of neutrons allow in-situ investigations at temperatures above room temperature using sample environments like furnaces or reaction chambers [19, 20, 22].

The authors performed several experiments to obtain information about parameters influencing the hydrogen solubility and diffusion as well as the correlation between stress and strain on one hand and hydrogen concentration and with it on hydrogen chemical potential on the other hand. The paper gives an introduction into neutron imaging and presents results of in-situ neutron radiography investigations on the inhomogeneous hydrogen uptake at a pre-cracked and strained sample of in- and ex-situ investigations of the hydrogen solubility and diffusion in the temperature range between 250 and 350 °C as well as ex-situ neutron radiography and tomography measurements at hydrogen pre-loaded three-point-

bending (3PB) bended at 870 and 600 °C under different conditions.

2 Determination of spatially resolved hydrogen concentration in zirconium alloys

In neutron imaging experiments usual variations in the attenuations of the neutron beam measured at detector different positions x,y result in the neutron image contrasts. The reciprocal of the attenuation, the transmission is described by the well-known Lambert-Beer law:

$$I(x,y) = I_0(x,y)e^{-\Sigma_{total}(x,y)s(x,y)} \quad (2)$$

I(x,y) and $I_0(x,y)$ are the intensities behind and before the sample (measured at detector pixel *x,y* with and without of the sample), Σ_{total} the total macroscopic neutron cross section at position *x,y* and *s* the path length of the neutrons through the sample at position *x,y*. Σ_{total} is the sum of the products of number density N_i and total microscopic neutron cross section σ_i of all isotopes *i* along the path of the neutron through the sample:

$$\Sigma_{total}(x,y) = \sum_i N_i(x,y)\sigma_i \quad (3)$$

The total neutron cross section of a hydrided zirconium alloys sample can be described as sum of total macroscopic neutron cross section of the alloy plus the total macroscopic neutron cross section of hydrogen.

$$\Sigma_{total}(x,y) = \Sigma_{total}^{Zry}(x,y) + N_H(x,y)\sigma_H \quad (3a)$$

On basis of Eq. (3a) the dependence of the total macroscopic cross section on the number density ratio of hydrogen to zirconium was determined experimentally using cladding segments with known hydrogen concentration. These calibration specimens were produced by annealing of the fresh cladding tube segments in Ar/H_2 atmosphere at various temperatures and hydrogen partial pressures [9]. Figure 1 compares the calibration measurements for the three neutron imaging facilities CoNRad (BENSC, Berlin, Germany), ANTARES (TU Munich, Garching, Germany) and ICON (Paul Scherrer Institut, Villigen, Switzerland) (an atomic ratio of $N_H/N_{Zr} = 1$ equals a mass concentration of 10930 wt.ppm). The differences are low because all three facilities use comparable cold neutron spectra.

3 In-situ measurements of the hydrogen uptake and redistribution in stressed samples at 350 °C

Processes related to DHC like hydrogen uptake and redistribution in mechanically pre-stressed specimens were tried to investigate in two measurement campaigns [23]. At first, pre-stressed specimens were annealed at 350 °C in Ar/H2 atmosphere. The Zircaloy-4 tensile samples with a thickness of 0.6 mm were strained using a steel/ceramics frame to apply the stress inside the INRRO furnace [22]. A neutron image sequence of this experiment is shown in Fig. 2. The hydrogen uptake was delayed by about 8 h. Obviously, the initial submicrometer thick oxide layer formed at room temperature during manufacturing, preparation and material storage had to be dissolved by diffusion of the oxygen into the bulk of the sample to enable hydrogen uptake. After this time, the

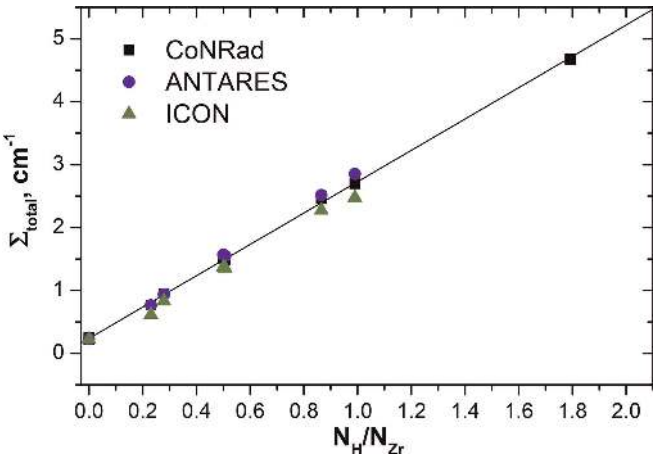

Fig. 1. Calibration of the dependence of the total macroscopic neutron cross section on the hydrogen to zirconium number density ratio for the CoNRad, ANTARES and ICON neutron imaging facilities

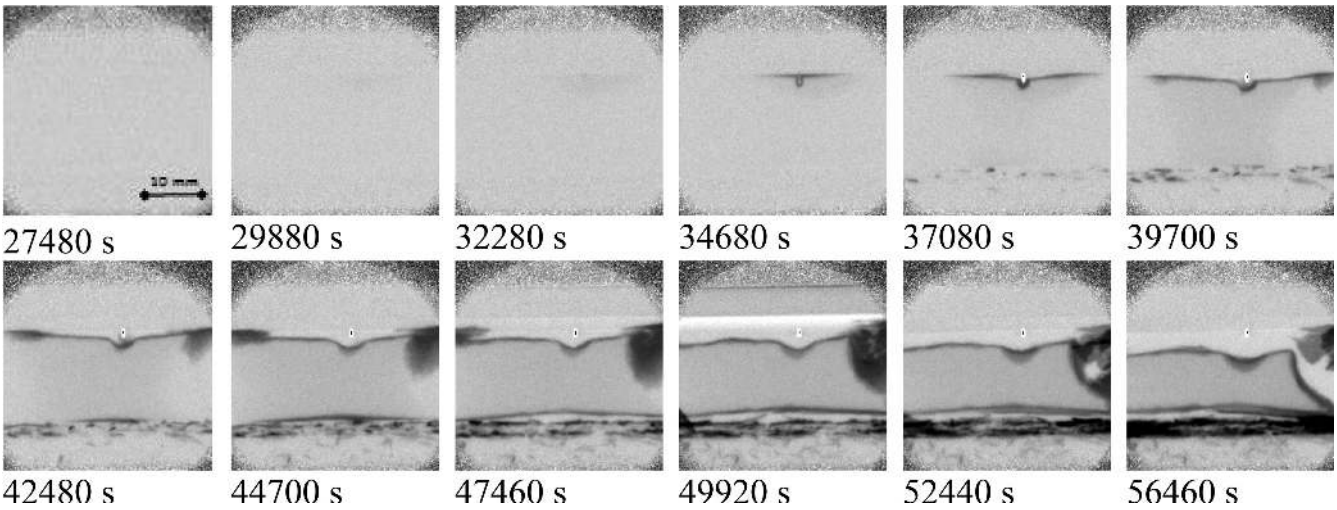

Fig. 2. Neutron radiograph sequence taken during the destruction of a mechanical stressed specimen in Ar/H_2 atmosphere at 350 °C (mechanical load in horizontal direction)

hydrogen absorption starts at notch position. After about 10 h the hydrogen is concentrated in the specimen region with the highest tensile stress (visible as slightly darker regions e. g. in the frames taken at 37 080 and 39 700 s). Spallation of small hydrides from the sample starts at the same time (dark objects below the specimen). Later, hot spots of the hydrogen uptake are formed. These dark hot spots characterized by very high hydrogen concentrations grow and result in additional breakaway of small hydrides from the sample until complete specimen destruction after about 15 h.

In a second beam-time the experiment was varied. The samples with a thickness of 6 mm were pre-oxidized. At both sides of the notch the oxide layer were removed to define the position of the hydrogen uptake. The samples were annealed again in Ar/H_2 atmosphere at 350 °C. The hydrogen uptake starts after about 4.5 h. This time was shorter than in the experiments before because the oxide at positions close to the notch was removed only about 40 min before the sample were put into the furnace with inert and reducing atmosphere. A fast hydrogen uptake follows. In order to prevent the complete destruction of the sample, the hydrogen supply was switched off after reaching a certain gray value in the radiograph at 17 000 s. In Fig. 3 examples of the radiograph sequence are given. The images are focused on the notch and pre-crack sample region after stopping the hydrogen supply the hydrogen distribution in the sample is changed very slowly as Fig. 4 shows for various vertical distances to the crack tip. The more or less stable hydrogen distribution demonstrates that nearly no diffusion occurred. This may happen if

a. the diffusion rate is very low or
b. the gradient in the chemical activity as the driving force for diffusion is low.

As will be shown later, hydrogen can diffuse quickly at this temperature. Therefore, the second reason is more probable. Ex-situ neutron tomography investigations of this sample were performed at the CoNRad facility. Figure 5 shows projections of the 3D reconstruction of the strongly hydrided areas. The hydrogen distribution along the notch is very heterogeneous as can be seen in the projections of the tomography reconstructions. High hydrogen concentrations were found at the sample surfaces where the notch ends. The flanks of the notch are not covered homogeneously by the hydrogen. On this basis it is hardly possible to extract data about the correlation between stress field ahead of the crack tip and hydrogen concentration. Measurement of hydrogen solubility and diffusion at temperatures of 250 to 350 °C

4 Measurement of hydrogen solubility and diffusion at temperatures of 250 to 350 °C

The spatially resolved hydrogen concentrations were measured with high precission in Zircaloy-2 (Zry-2) and Zr-

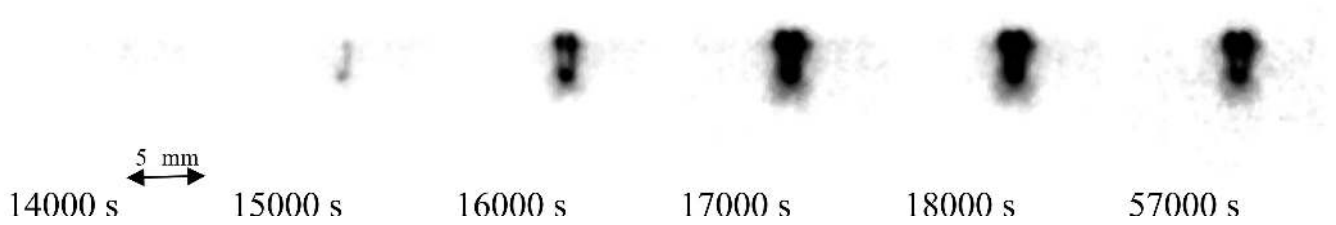

Fig. 3. Neutron radiograph sequence taken during hydrogen loading in Ar/H_2 atmosphere until 18 000 s and inert annealing of a mechanical stressed specimen until 57 000 s at 350 °C

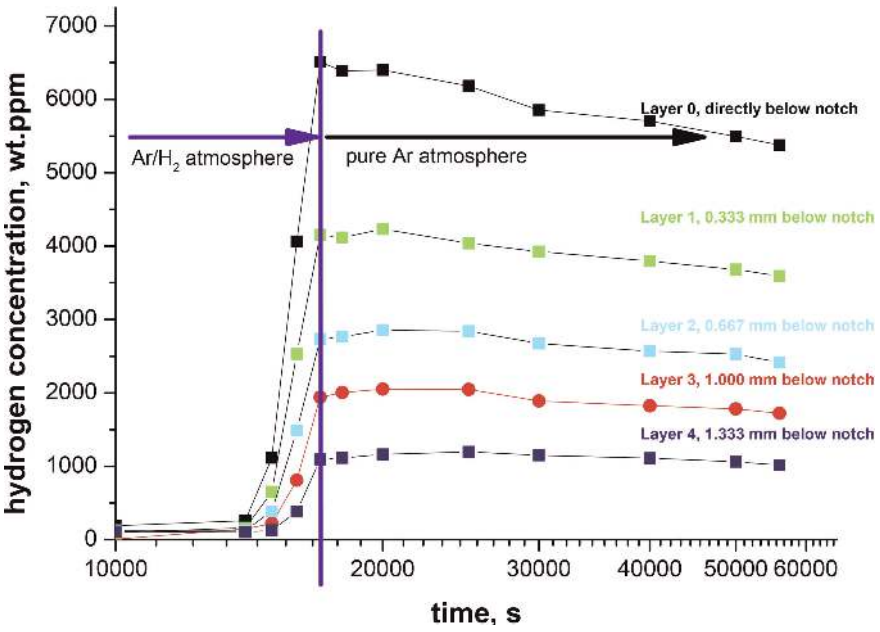

Fig. 4. Time dependence of the averaged hydrogen concentrations at various distances from the crack tip

2.5 %Nb specimens coated with a Zr hydride layer after annealing between 250 and 350 °C for various thermo-mechanical treatments [21]. The temperature dependence of hydrogen solubility and diffusion were extracted by these investigations.

Figure 6 compares the hydrogen distributions after annealing at temperatures of 250, 300 and 350 °C for rolling and normal direction of a rolled Zr-2.5 %Nb plate, heat treated at 860 °C for 3 h prior to formation of the hydride layer, as an example. At position 0 – the interface to the Zr hydride layer the hydrogen solubility is measured. It does not differ between the two rolling plate directions for this material. The hydrogen solubility of Zry-2 seems to be slightly higher in normal direction than in rolling direction or in Zr-2.5 %Nb. However, the differences are very small. A stress release pre-annealing does not change the solubility noticeably.

The distributions were fitted by the diffusion law of Eq. (4) derived from Fick's law for constant hydrogen activity at the

Fig. 5. Projection of the 3D reconstructed hydrogen distribution along the notch over the whole sample width obtained from the neutron tomography measurements (the width of the sample is 6 mm)

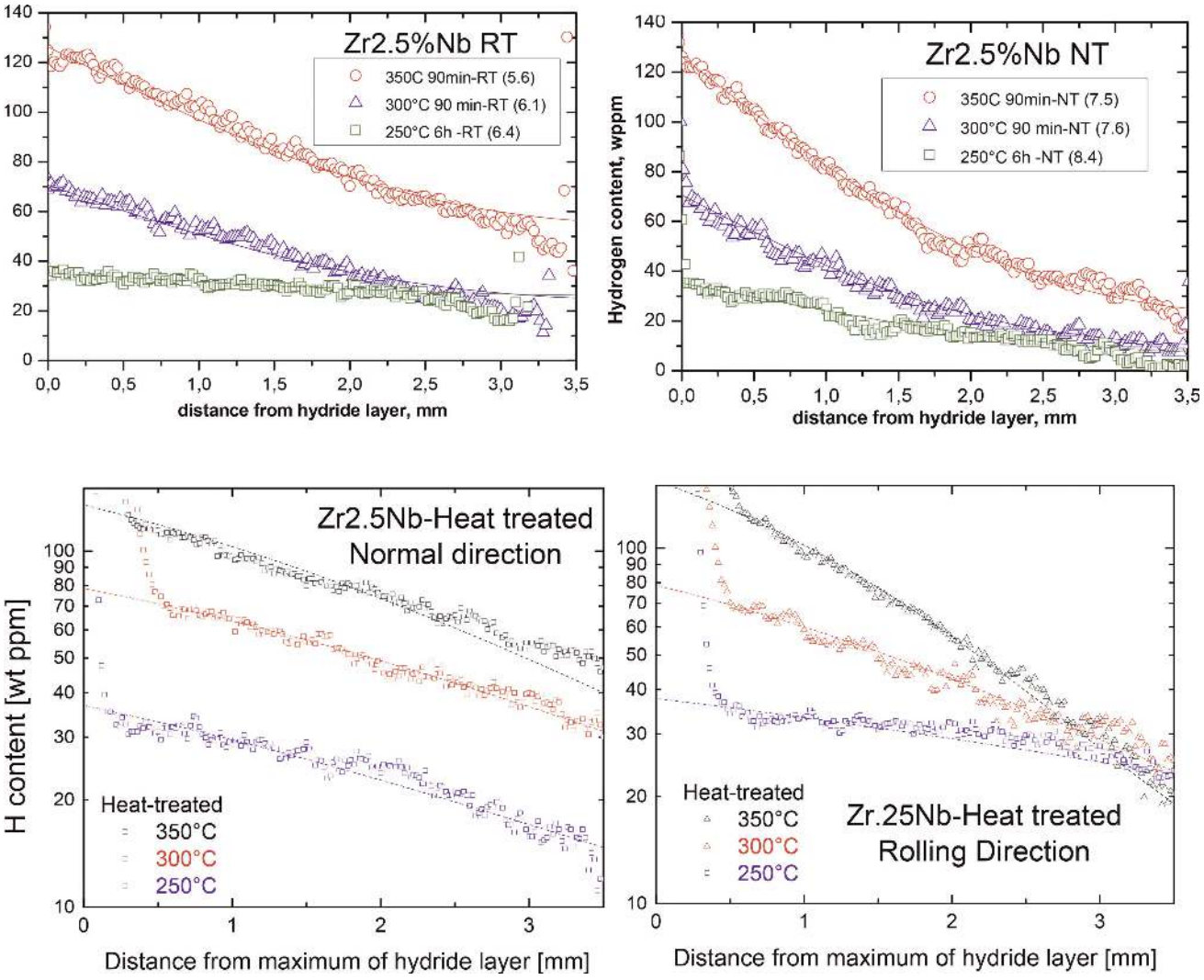

Fig. 6. Comparison of the hydrogen distribution after annealing at 250, 300 and 350 °C for rolling and normal direction of the rolled Zr-2.5 %Nb plate

opposite side of the interface. This presumption is valid, as long the hydride layer at the sample is not completely consumed.

$$c(x,t) = c_0\left(1 - erf\left\{\frac{x}{2\sqrt{Dt}}\right\}\right) \quad (4)$$

x is the distance to the interface, t the time, c_0 the concentration at the interface and D the diffusion coefficient. Figure 7 compares the temperature dependences of the diffusion coefficient determined by fitting the hydrogen distribution for the two alloys and two thermo-mechanical pre-treatments. The temperature is given in equal distant 1/T steps according to the Arrhenius law. The hydrogen diffusion is faster in the Zr-2.5 %Nb alloy than in Zry-2. The reason for it seems to be the remaining β-Zr phase at grain boundaries in the niobium-containing alloy in hydrogen diffusion occurs much faster than in the tin containing alloy. The diffusion is faster in rolling direction than in normal direction for Zry-2 but opposite for the heat-treated Zr-2.5 %Nb. For the Zry-2 the elongated grains in rolling direction resulting in enhanced grain boundary diffusion can explain the effect. In the Zr-2.5 %Nb the continuous β-Zr network can be broken by the plastic deformation occurring mostly in rolling direction. In this case the preferred diffusion path would be also interrupted.

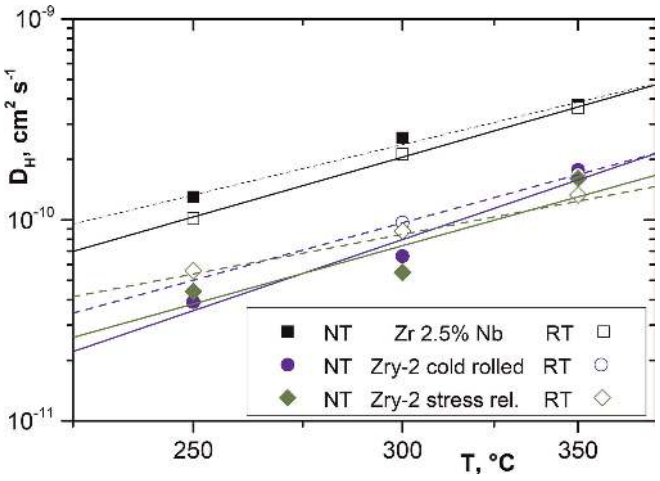

Fig. 7. Temperature dependence of the hydrogen diffusion coefficient for the different materials and thermos-mechanical treatments

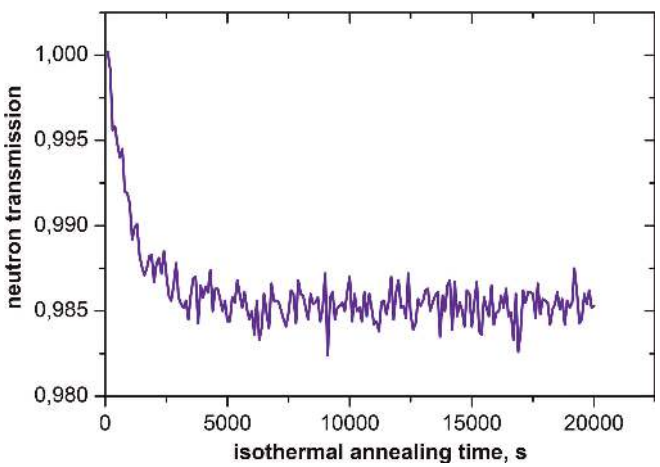

Fig. 8. Development of the neutron transmission at a distance to the hydride layer of ~3.25 mm during isothermal annealing at 280 °C

The tests also comprised in-situ neutron radiography measurements of the hydrogen diffusion. However, they were not successful. The neutron radiographs have to refer to the sample at test temperature at the very beginning of the annealing to suppress the effect of sample holder or temperature caused changes of the position of furnace structure elements. Even very small position changes less than a pixel size (about 20 µm) hint a successful referencing. Because of the heating rate of 10 K/min a certain hydrogen re-distribution occurs already during heatup to 280 °C. Figure 8 plots the neutron transmission vs time of isothermal annealing at 280 °C. The transmission was measured at a position opposite to the hydride layer in a distance of about 3.5 mm from the hydride/Zry-2 interface. The plot shows that after about 50 min annealing time (plus the 25 min heat up time) equilibrium is established. No further changes in the neutron transmission caused by hydrogen diffusion occur because the hydrogen concentration was homogenized over the whole sample. It demonstrates how fast is hydrogen diffusion even at the relative low temperature of 280 °C.

5 Measurement of the hydrogen distribution at a 3PB specimen after bending at 600 °C

The aim of this feasibility study was the measurement of the hydrogen concentration in dependence on stress/strain in Zircaloy-4 samples. Four of the five specimens with dimensions of 35 mm × 4 mm × 3 mm were preloaded with hydrogen to concentrations of about 1 000 to 1 100 wt · ppm. Specimen HRD0 was kept as reference. The samples were oxidized in steam to catch the hydrogen in the sample by forming an oxide layer. Three-point-bending (3PB) tests were performed at temperatures of 860 °C (HRD-1 and -2) and 600 °C (HRD-3 and -4). The load was increased until a derivation from the linear elastic behavior occurred. Then the load was kept constant for various times. Finally, the samples were cooled down in the furnace keeping the mechanical load constant. Figure 9 shows a neutron radiograph of these samples. The darker regions at both sides come from the glue band fixing the samples.

The specimen HRD4 shows a clear gradient in the neutron transmission and with it in the hydrogen concentration in the direction of the mechanical load (vertical z axis) as can be

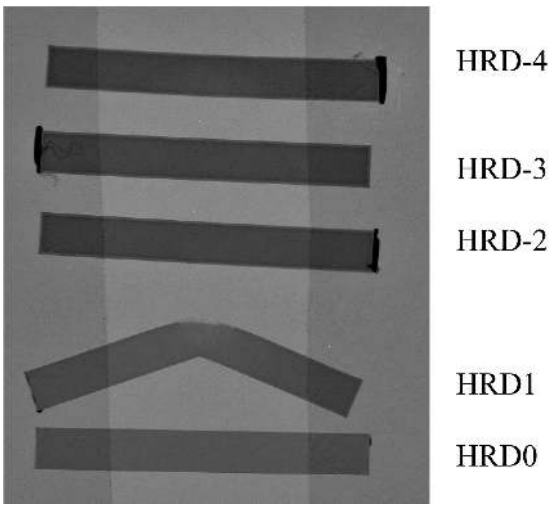

Fig. 9. Neutron radiograph of the HRD specimens

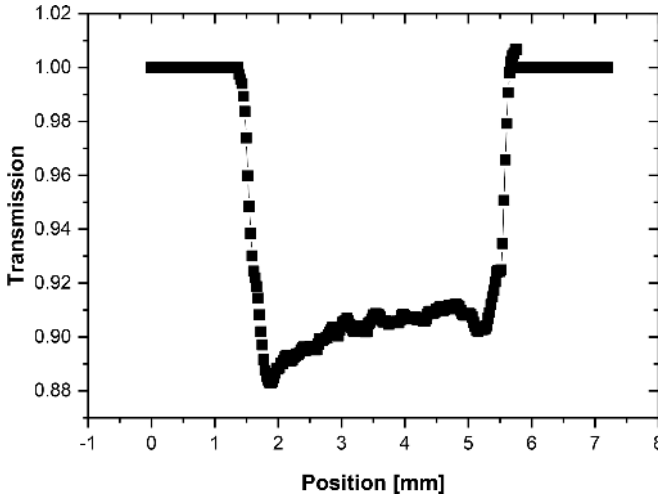

Fig. 10. Dependence of the neutron transmission the z position at sample HRD4

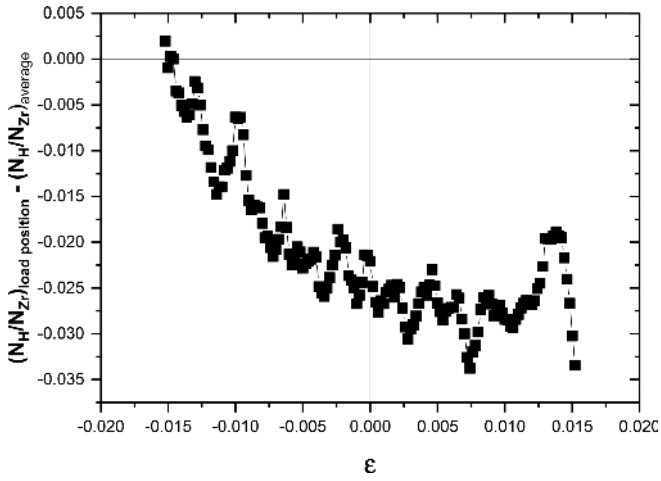

Fig. 11. Correlation between the number density ratio between hydrogen and zirconium and the elastic strain at the mechanical load position of sample HRD4

seen in Fig. 10. Assuming pure elastic deformation the z dependence of the strain can be estimated. Figure 11 plots the ratio between the number densities of hydrogen and zirconium vs. the elastic strain estimated. The curve contradicts the expectations based on the well-known effect that hydrogen solubility increases with increasing elastic tensile strain. The values of the hydrogen concentration at this axial position of the mechanical load are below the mean value determined at positions far away from this position. Obviously, hydrogen release occurs at the highest loaded position through the surface exposed to the highest tensile stress and strain.

It must be concluded that the experiments were not successful. New experiments have to be designed to measure the correlation between stress/strain and hydrogen concentration and with it the stress dependence of the chemical potential of hydrogen in zirconium alloys.

6 Conclusion and outlook

The investigations already performed demonstrate that neutron imaging is a powerful tool to study hydrogen uptake, diffusion and distribution in zirconium alloys. In particular, the measurements of maximal hydrogen solubility and diffusion were very successful. The determination of the correlation between stress/strain and hydrogen concentration and with it the stress/strain dependence of the chemical potential of hydrogen in zirconium alloys was not yet achieved. New experiments have to be designed and performed to reach this goal. May be that new methodical developments like neutron microscopy providing spatial resolutions down to several micrometer will provide better possibilities to measure the unknown correlations and to investigate DHC directly.

Acknowledgements

The investigations were performed at the ICON facility at the Swiss neutron source SINQ (Paul Scherrer Institute Villigen, Switzerland), at the ANTARES facility at the Munich research reactor FRM2 (Techn. Univ. Munich, Garching, Germany) and at the CoNRad facility at the Berlin research reactor (Helmholtz Centre Berlin, Germany). The authors thank for providing beam-time and for technical support.

(Received on 28 May 2018)

References

1 *Mills, J. W.; Huang, F. H.*: Delayed Hydride Cracking Behavior for Zircaloy-2 Plate. Engineering Fracture Mechanics 39 (1991) 241, DOI:10.1016/0013-7944(91)90040-8
2 *Varias, A. G.*: Mathematical Model for Hydrogen Diffusion, Energy Flow and Hydride Formation in Zirconium under Stress. Solid Mechanics Research Office, BR-04-10-98, 1998
3 *Varias, A. G.; Massih, A. R.*: Hydride-Induced Embrittlement in Metals – Stress and Temperature Effects. In: Ståhle P., Sundin K.G. (eds.) IUTAM Symposium on Field Analyses for Determination of Material Parameters – Experimental and Numerical Aspects. Solid Mechanics and its Applications, vol 109. Springer, Dordrecht (2003)
4 *IAEA*: Delayed hydride cracking in zirconium alloys in pressure tube nuclear reactors, *Final report of a coordinated research project 1998–2002, IAEA-TECDOC-1410 (2004)*
5 *Kim, Y. S.*: Driving Force for Delayed Hydride Cracking of Zirconium Alloys. Metals & Materials International 11 (2005) 29, DOI:10.1007/BF03027481
6 *IAEA*: Delayed Hydride Cracking of Zirconium Alloy Fuel Cladding. final report of a coordinated research project 2005–2009. IAEA-TECDOC-1649 (2010)
7 *McRae, G. A.; Coleman, C. E.; Leitch, B. W.*: The first step for delayed hydride cracking in zirconium alloys. J. Nucl. Mater. 396 (2010) 130, DOI:10.1016/j.jnucmat.2009.08.019
8 *IAEA*: Evaluation of Conditions for Hydrogen Induced Degradation of Zirconium Alloys during Fuel Operation and Storage. Final Report of a Coordinated Research Project 2011–2015, IAEA-TECDOC-1781 (2015)
9 *Grosse, M.; Lehmann, E.; Vontobel, P.; Steinbrueck, M.*: Quantitative determination of absorbed hydrogen in oxidised zircaloy by means of neutron radiography. Nucl. Instr. & Methods in Phys. Res. Vol A 566 (2006) 739–745
10 *Gröschel, F.; Schleuniger, P.; Hermann, A.; Lehmann, E.*: Neutron radiography of irradiated fuel rod segments at the SINQ: Loading, transfer and irradiation concept. Nucl. Instr. & Meth. A 424 (1999) 215, DOI:10.1016/S0168-9002(98)01251-0
11 *Yasuda, R.; Matsubayashi, M.; Nakata, M.; Harada, K.*: Application of neutron radiography for estimating concentration and distribution of hydrogen in Zircaloy cladding tubes. J. Nucl. Mater. 302 (2002) 156, DOI:10.1016/S0022-3115(02)00778-X
12 *Lehmann, E.; Vontobel, P.; Hermann, A.*: Non-destructive analysis of nuclear fuel by means of thermal and cold neutrons. Nucl. Instr. Meth. A 515 (2003) 745, DOI:10.1016/j.nima.2003.07.059

13 *Wang, Z.; Garbe, U.; Li, H.; Harrison, R. P.; Kaestner, A.; Lehmann, E.*: Observations on the zirconium hydride precipitation and distribution in Zircaloy-4. Metallurg. & Materials Trans. B02/2014 (2014) 532
14 *Smith, T.; Bilheux, H.; Ray, H.; Bilheux, J. C.; Yan, Y.*: High Resolution Neutron Radiography and Tomography of Hydrided Zircaloy-4 Cladding. Materials Phys. Proc. 69 (2015) 478, DOI:10.1016/j.phpro.2015.07.067
15 *Grünzweig, C.; Mannes, D.; Kaestner, A.; Schmid, F.; Vontobel, P.; Hovind, J.; Hartmann, S.; Peetermans, S.; Lehmann, E.*: Progress in Industrial Applications using Modern Neutron Imaging Techniques. Phys. Proc. 43 (2013) 231, DOI:10.1016/j.phpro.2013.03.027
16 *Tremsin, A. S.; Morgano, M.; Panzner, T.; Lehmann, E.; Filgers, U.; Vallerga, J. V.; McPhate, J. B.; Siegmund, O. H. W.; Feller, W. B.*: High resolution neutron imaging capabilities at BOA beamline at Paul Scherrer Institut. Nucl. Instrm. & Meth. A784 (2015) 486, DOI:10.1016/j.nima.2014.09.026
17 *Abolhassani, S.; Bart, G.; Bertsch, J.; Degueldre, C.; Grosse, M.; Hallstadius, L.; Hermann, A.; Kuri, G.; Ledergerber, G.; Lemaignan, C.; Martin, M.; Portier, S.; Proff, C.; Restani, R.; Valance, S.; Valizadeh, S.; Wiese, H.*: Corrosion and hydrogen uptake in zirconium claddings irradiated in light water reactors. Zirconium in the Nuclear Industry: 17th Volume, Eds. Comstock B. and Barbéris P., ASTM-STP1543 (2015)
18 *Brachet, J.-C.; Hamon, D.; Le Saux, M.; Vandenberghe, V.; Toffolon-Masclet, C.; Rouesne, E.; Urvoy, S.; Béchade, J.-L.; Raepsaet, C.; Lacour, J.-L.; Bayon, G.; Ott, F.*: Study of secondary hydriding at high temperature in zirconium based nuclear fuel cladding tubes by coupling information from neutron radiography/tomography, electron probe micro analysis, micro elastic recoil detection analysis and laser induced breakdown spectroscopy microprobe. J. Nucl. Mater. 488 (2017) 267–286, DOI:10.1016/j.jnucmat.2017.03.009
19 *Grosse, M.; Steinbrück, M.; Schillinger, B.; Kaestner, A.*: In-situ investigations of the hydrogen uptake of zirconium alloys during steam oxidation, 18th Intern. ASTM Symp. on Zirconium in the Nucl. Ind., May 15–19 2016, Hilton Head Island SC (USA), DOI:10.1520/STP159720160041
20 *Makowska, M. G.; Theil Kuhn, L.; Cleemann, L. N.; Lauridsen, E. M.; Bilheux, H. Z., Molaison, J. J.; Santodonato, L. J.; Tremsin, A. S.; Grosse, M.; Morgano, M.; Kabra, S.; Strobl, M.*: Flexible sample environment for high resolution neutron imaging at high temperatures in controlled atmosphere. Rev. Sci. Instr. 86 (2015) 125109, PMid:26724075; DOI:10.1063/1.4937615
21 *Buitrago, N. L.; Santisteban, J.R.; Tartaglione, A.; Marín, J.; Barrow, L.; Daymond, M.R.; Schulz, M.; Grosse, M.; Tremsin, A.; Lehmann, E.; Kaestner, A.; Kelleher, J.; Kabra, S.*: Determination of very low concentrations of hydrogen in zirconium alloys by neutron imaging. J. Nucl. Mater. 503 (2018) 98, DOI:10.1016/j.jnucmat.2018.02.048
22 *Grosse, M.; Van Den Berg, M.; Goulet, C.; Lehmann, E.; Schillinger, B.*: In-situ neutron radiography investigations of hydrogen diffusion and absorption in zirconium alloys. Nucl. Instr. & Meths in Phys. Res. A: Accelerators, Spectrometers, Detectors and Associated Equipment 651 (2011) 253, DOI:10.1016/j.nima.2010.12.070
23 *Grosse, M.*; *Valance, S.; Stuckert, J.; Steinbrueck, M.; Walter, M.; Kaestner, A.; Hartmann, S.; Santisteban, J.*: Neutron Imaging Investigations of the Hydrogen Related Degradation of the Mechanical Properties of Zircaloy-4 Cladding Tubes. MRS online proceedings library archive 1528 (2013), DOI:10.1557/opl.2013.364

The authors of this contribution

Mirco Grosse (corresponding author)
E-mail: Mirco.Grosse@KIT.edu
Karlsruhe Institute of Technology
P.O. Box 3640
76021 Karlsruhe
Germany

Javier Roberto Santisteban
Centro Atómico Bariloche-CNEA and CONICET
Av Bustillo Km 9.500
Bariloche 8400
Argentina

Dr. *Dr. Johannes Bertsch*
Paul Scherrer Institut
5232 Villigen PSI
Switzerland
johannes.bertsch@psi.ch

Dr. *Burkhard Schillinger*
Technische Universität München
James-Franck-Str. 1
85748 Garching
Germany
burkhard.schillinger@tum.de

Dr. *Anders Kaestner*
Paul Scherrer Institut
5232 Villigen PSI
Switzerland
Anders.kaestner@psi.ch

Mark Richard Daymond
Department of Mechanical and Materials Engineering
Queens University,
Nicol Hall, 60 Union Street
Kingston, K7L 3N6
Canada

Dr. *Nikolay Kardjilov*
Helmholtz Zentrum Berlin
Hahn-Meitner-Platz 1
14109 Berlin
Germany

Bibliography
DOI 10.3139/124.110946
KERNTECHNIK
83 (2018) 6; page 495–501

ISSN 0932-3902